Journal of Asian Earth Sciences 134 (2017) 63–71

Contents lists available at ScienceDirect

Journal of Asian Earth Sciences

journal homepage: www.elsevier.com/locate/jseaes

Full length Article

A ubiquitous hydrothermal episode recorded in the sheet-crack cements of a Marinoan cap dolostone of South China: Implication for the origin of the extremely ^{13}C-depleted calcite cement

Guanghong Zhou [a,b], Taiyi Luo [a,*], Mingzhong Zhou [c], Lecai Xing [d], Tian Gan [a,b]

[a] State Key Laboratory of Ore Deposit Geochemistry, Institute of Geochemistry, Chinese Academy of Sciences, Guiyang 550002, China
[b] University of Chinese Academy of Sciences, Beijing 100049, China
[c] School of Geographical and Environmental Sciences, Guizhou Normal University, Guiyang 550001, China
[d] School of Earth Science and Engineering, Hebei University of Engineering, Handan 056038, China

ARTICLE INFO

Article history:
Received 20 June 2016
Received in revised form 2 November 2016
Accepted 3 November 2016
Available online 4 November 2016

Keywords:
Fluid inclusion
Sheet-crack cement
Cap carbonate
Jiulongwan section

ABSTRACT

Sheet-crack – primarily filled with chalcedony, quartz and calcite – is a type of significant sedimentary structure in almost all documented cap carbonates in platform-to-slope settings, which sharply overlie the global Marinoan (~635 Ma) glacial tillite. The Jiulongwan section, located in the Yangtze Gorges areas, South China, is significant for the first discovery of extremely ^{13}C-depleted ($\delta^{13}C$ down to −41‰) calcite cements in sheet-crack structure (Jiang et al., 2003a), which provides direct evidence for the methane seep hypothesis (Kennedy et al., 2001). Focusing on the calcite cements in the same section, Bristow et al. (2011) proposed a hydrothermal origin based on high temperatures (378 °C) determined by carbonate clumped isotope thermometry (CCIT). In this study, we provide evidence for the hydrothermal model using fluid inclusion technology (FIT) to quartz cements in the Jiulongwan section. The widespread sheet-crack structures in South China have uniform mineral paragenetic assemblages, which apparently reflect three stages of a hydrothermal fluid activity, including dolomitization at the early stage, silicification comprising chalcedony and quartz at the middle stage, and calcitization characterized by carbonaceous calcite filling preexisting voids at the late stage. Primary aqueous fluid inclusions from quartz crystals have homogenization temperatures of approximately 160–220 °C (mean, 192 °C, n = 31), while the salinity histogram contains two peaks at low salinity (6.3–8.3 wt.% NaCl equiv.) and high salinity (18.0–20.8 wt.% NaCl equiv.), reflecting precipitation caused by mixing of high- and low-salinity fluids. A modified and detailed hydrothermal model is proposed indicating that the sheet-crack structure resulted from successive thermal fluid activity after karstic dissolution due to postglacial isostatic rebound. This model is compatible with the unified sequence of glacio-eustatic events after the termination of Marinoan glaciation (Zhou et al., 2010) and the temperature results determined by CCIT (Bristow et al., 2011).

1. Introduction

Globally, most Neoproterozoic Marinoan glacial deposits (~635 Ma) (Condon et al., 2005) are directly overlain by meter- to decameter-scale (Liu et al., 2014) cap carbonates. These cap carbonates are characterized by anomalous ^{13}C-depleted and enigmatic sedimentary structures including tepee-like features, stromatactis-like cavities, layer-parallel sheet-cracks, and cemented breccia (Jiang et al., 2003a, 2006a; Wang et al., 2008). These distinctive sedimentary structures are closely related to severe climatic oscillations and perturbations of the oceanic chemical environment after Marinoan deglaciation. Previous research has revealed that the termination of Marinoan glaciation on the Yangtze Block was followed by a series of glacio-eustatic events (Zhou et al., 2010): (1) deglaciation and associated transgression in the early stage that resulted in rapid deposition of cap carbonate; (2) isostatic rebound that induced quick crustal uplift and relative sea level fall (Hoffman and Macdonald, 2010), leading to karstic dissolution of cap carbonate; and (3) a second, larger-scale glacio-eustatic transgression at the late stage.

* Corresponding author.
E-mail address: luotaiyi@vip.gyig.ac.cn (T. Luo).

http://dx.doi.org/10.1016/j.jseaes.2016.11.007
1367-9120/

One of the most idiosyncratic lithological features of Marinoan cap carbonate is the presence of sheet-crack cement structure, which is typically confined near the base of almost all documented cap carbonates in a platform-to-slope setting, such as cap carbonates on the Congo and Kalahari cratons of Namibia (Hoffman et al., 2007; Hoffman and Macdonald, 2010) and the Taoudeni Basin (Shields et al., 2007) in Africa, the Kimberley region of northwestern Australia (Corkeron, 2007), the Yangtze Block of South China (Jiang et al., 2006a; Xiao et al., 2012) and so on. Marinoan cap carbonate in South China is well-exposed, and it is one of the most intensively investigated Neoproterozoic successions in the world. Cap carbonate with consistent sheet-crack cement structure is traceable for at least 350 km from platform to slope settings of the Yangtze Block. Typically, it is well outcropped at the Jiulongwan, Huajipo, Xiaofenghe, Daping, Tianping, Songlin, Wenghui sections (Jiang et al., 2006a, 2011; Xiao et al., 2012). The widespread sheet-crack structure in the cap carbonate has a uniform mineral paragenetic sequence: it starts with re-crystallized dolomite, which is followed by siliceous minerals (chalcedony and quartz), and ends with later stage calcite.

To explain the genesis of the enigmatic sheet-crack structure, several models have been proposed. One hypothesis suggests that the structure is caused by destabilization of methane hydrate (Kennedy et al., 2001; Jiang et al., 2003a, 2006b). An important piece of evidence for this hypothesis is the extremely ^{13}C-depleted gray calcite in sheet-crack from the Doushantuo cap carbonate at the Jiulongwan ($\delta^{13}C$ down to $-41‰$), Wangzishi and Huajipo ($\delta^{13}C$ down to $-48‰$) sections (Jiang et al., 2003a; Wang et al., 2008). Some workers ascribe the structure to pore-fluid overpressure driven by the rapid crustal uplift and transient sea level fall associated with isostatic rebound (Hoffman and Macdonald, 2010) or by expansion in early diagenetic dolomite cementation (Gammon, 2012; Gammon et al., 2012). A hydrothermal origin has also been invoked based on CCIT evidence, which determined average temperature of 112 °C for the recrystallized dolomite, 156 °C for the late stage calcite spar, and 378 °C for the highly ^{13}C-depleted gray calcite cements in the sheet-crack structure from the Jiulongwan section (Bristow et al., 2011). Evidence for the effects of hydrothermal fluids is also indicated by the relatively high $^{87}Sr/^{86}Sr$ isotope ratios from dolomicrite and white calcite spar and the chloritization of saponite at the base of the Doushantuo Formation (Bristow et al., 2011; Derkowski et al., 2013). Moreover, an external origin for post-depositional fluids, relative to depositional fluid, has also been proposed by some workers based on the distinct differences in stable isotopes and trace element compositions between veins (partly sheet-crack cements) and cap carbonate wallrock (Zhao and Zheng, 2013, 2015).

However, there is still a lack of unambiguous data concerning the nature of the hydrothermal activity, although it should be preserved in fluid inclusions. Fluid inclusions are common and inherent features of minerals precipitated from fluid, in which the temperature and salinity of the paleo-fluid can be recorded. FIT is a widely used geochemical technique for determining the thermobaric and chemical evolution of geological systems, and the temperatures and salinities measured by fluid inclusions have been verified by many oregeochemistry experiments. Therefore, the above genetic models can be clarified by FIT research. We would expect a typical low temperature close to submarine temperatures (<10 °C) for the methane-seep model and a stable salinity for the pore-fluid overpressure model. However, a well-defined 160–220 °C homogenization temperature and two salinity peaks have been observed in quartz from sheet-crack cements. Combined with a detailed mineral paragenetic sequence, a modified hydrothermal origin model of sheet-crack cements formation is developed in this paper.

2. Geological background

Neoproterozoic successions are well-exposed in the Yangtze Gorges area, especially the Jiulongwan section (Fig. 1a–c), which is the type section of early Ediacaran succession in China (Jiang et al., 2003b; McFadden et al., 2008; Xiao et al., 2012; Du et al., 2015). The Yangtze Gorges area is located in the northern Yangtze Block which is adjacent to the northwest of the Cathaysia Block (Jiang et al., 2003b; Wang and Li, 2003; Shen et al., 2011). During the break-up of Rodinia, a passive continental margin and a number of sub-basins were formed in the southeastern margin of the Yangtze Block (Wang and Li, 2003). After the termination of the Marinoan glaciation, transgressive seawater inundated the Yangtze platform, resulting in the formation of basin, slope and platform facies successively from southeast to northwest.

The Ediacaran successions are composed of the Doushantuo Formation and the overlying Dengying Formation at the Jiulongwan section. The Doushantuo Formation consists of four lithostratigraphic members (Zhou and Xiao, 2007; Zhou et al., 2012; Du et al., 2015). Member I (approximately 5 m thick) predominately contains dolomicrite, dubbed "cap dolostone", which directly overlies the Nantuo glacial diamictite and is characterized by anomalous ^{13}C-depletion and distinctive sedimentary structures. The overlying Member II (approximately 70 m thick) is mainly composed of black shale interbedded with dark gray, finely crystalline, and thin-bedded dolostone, and certain parts contain abundant peasized fossiliferous chert nodules. Member III (approximately 70 m thick) represents medium- to thick-bedded dolostone intercalated with irregular chert strips and nodules, containing abundant microfossils (Yin et al., 2007). Member IV (approximately 10 m thick) is characterized by organic-rich mudstone, black shale and abundant huge calcareous concretions and lenticles. According to the sedimentological characteristics, the cap carbonates can be divided into three distinct units (Jiang et al., 2006a, 2006b; Wang et al., 2008). Unit C1 (1–1.5 m thick), at the base of the cap carbonate, contain massive dolomicrite and presents enigmatic sedimentary structures. The middle layer Unit C2 (approximately 2 m thick) is laminated dolomicrite and dolomitic limestone with local tepee-like structures. The uppermost part Unit C3 (approximately 1.5 m thick) is composed of thinly-laminated, silty limestone and dolostone.

3. Sampling and analytical techniques

3.1. Sampling

Two samples that contain typical sheet-crack cements were collected from unit C1 of the cap carbonates in the Doushantuo Formation at the Jiulongwan section. The sheet-cracks are planar opening and bedding-parallel (sometimes cross-cutting) extension cracks and are filled with isopachous cements (0.7–2 cm thick). Two stages of mineral assemblages in sheet-crack cements are observed from hand-specimen: the early stage siliceous minerals (composed of fibrous or radial chalcedony, micro-quartz and mega-quartz) and the later stage calcite (Fig. 1d). Two petrographic slices and four doubly polished fluid inclusion slices were prepared from the samples.

3.2. Fluid inclusion analytical method

According to the criteria proposed by Roedder and Ribbe (1984), only the primary or pseudosecondary inclusions should be selected for microthermometric analysis (MTA). MTA has been performed on a Linkam THMGS600 heating–freezing stage attached to a Leica microscope, and temperature in the stage has been calibrated with

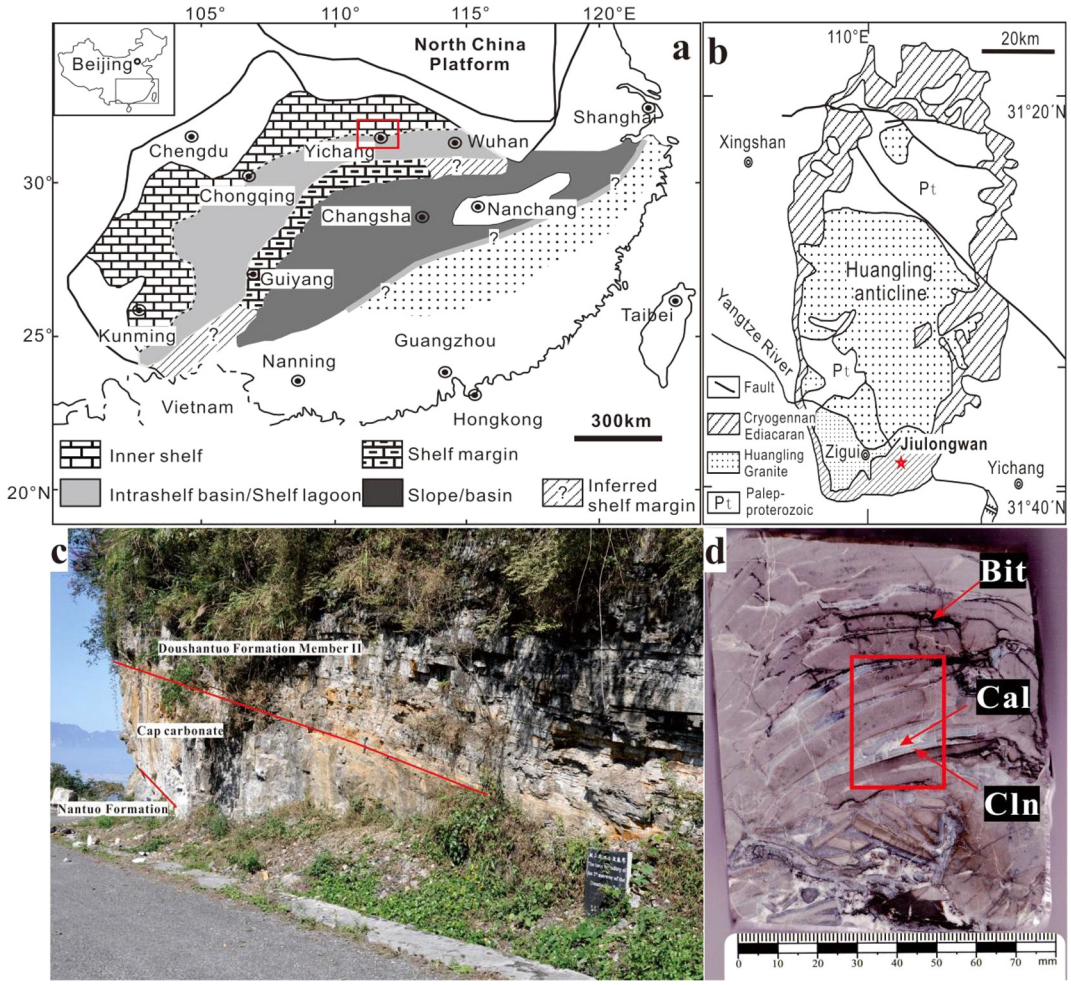

Fig. 1. (a) A generalized paleogeographic reconstruction for the Yangtze platform during the Doushantuo deposition (Jiang et al., 2011). (b) Simplified geological map of the Yangtze Gorges area (Zhao et al., 1985), showing locations (five-pointed star) of the Jiulongwan section. (c) Field photograph of the Doushantuo cap carbonates at the Jiulongwan section in the Yangtze Gorges area, showing lithostratigraphic sequences. (d) Scanned image of sample containing sheet-crack cements collected from the Jiulongwan section. Red box shows area of thin section. The minerals of sheet-crack cements include early-stage siliceous minerals and later-stage calcite (Bit: bitumen; Cal: calcite; Cln: chalcedony). (For interpretation of the references to color in this figure legend, the reader is referred to the web version of this article.)

synthetic pure H_2O fluid inclusions (0 and +374.1 °C) and synthetic pure CO_2 fluid inclusions (−56.6 °C). The uncertainty of temperature measurements is ±0.1 °C below 0 °C, and ±1 °C above 0 °C. Vapor and liquid compositions of individual fluid inclusions have been analyzed by a Renishaw Via Reflex laser Raman spectroscope.

The eutectic temperature (T_e), the freezing point temperature (T_m) and the homogenization temperature (T_h) of fluid inclusions were determined from temperatures of phase changes during MTA. Selected fluid inclusions were cooled until frozen completely to a glassy solid and then were heated slowly. The glassy solid (hydrohalite) decomposed to produce a fine-grained mixture of hydrohalite and ice at T_e (T_e is usually very hard to detect. In this study, it was measured in only some of the inclusions.). With slight heating above T_e, the hydrohalite disappeared, and the ice recrystallized to large crystals. With continued heating, the ice crystals gradually dissolved, and the temperature of the last ice melting was defined as the T_m of the inclusion. With further heating, the vapor bubble of the fluid inclusion disappeared at T_h. Specifically, the heating rate should be reduced to less than 0.1 °C/min near T_m and T_h. Salinity was calculated from T_m according to the methodology of Bondar (1993) and Chi and Ni (2007). All of the experiments were conducted at the State Key Laboratory of Ore Deposit Geochemistry, Institute of Geochemistry, Chinese Academy of Sciences.

4. Results

4.1. Paragenetic sequence of minerals

The widespread sheet-crack structure in cap dolostone from South China has uniform mineral paragenetic sequence. From the primary cap dolostone into the sheet-crack structure, the dolomite grains gradually re-crystallize from fine to coarse, accompanied with reduction of organic carbon. The primary cap dolostone, is gray colored on fresh surfaces, and is mainly composed of carbonaceous microcrystalline dolomite (crystal size <15 μm, mostly 5–10 μm). The transition zone consists of grayish finely crystalline dolomite (<40 μm, mostly 15–30 μm) (Fig. 2a). Adjacent to sheet-cracks, the dolomites are intensely recrystallized to euhedral, coarse-grained spar (mostly 300–500 μm), occasionally accompanied with barite in platform facies.

The cements that filled in sheet-cracks typically contain the early stage siliceous minerals (chalcedony and quartz) and the later stage calcite. In certain thin sheet-cracks, the cements are chalcedony only or chalcedony plus quartz. In thick sheet-cracks, the complete mineral sequence starts with fibrous chalcedony parallel to the vein edge, follows by euhedral quartz (Fig. 2b), and ends with later stage organic-rich calcite filling in the remaining spaces. Chalcedony commonly has an obvious laminated texture, and most

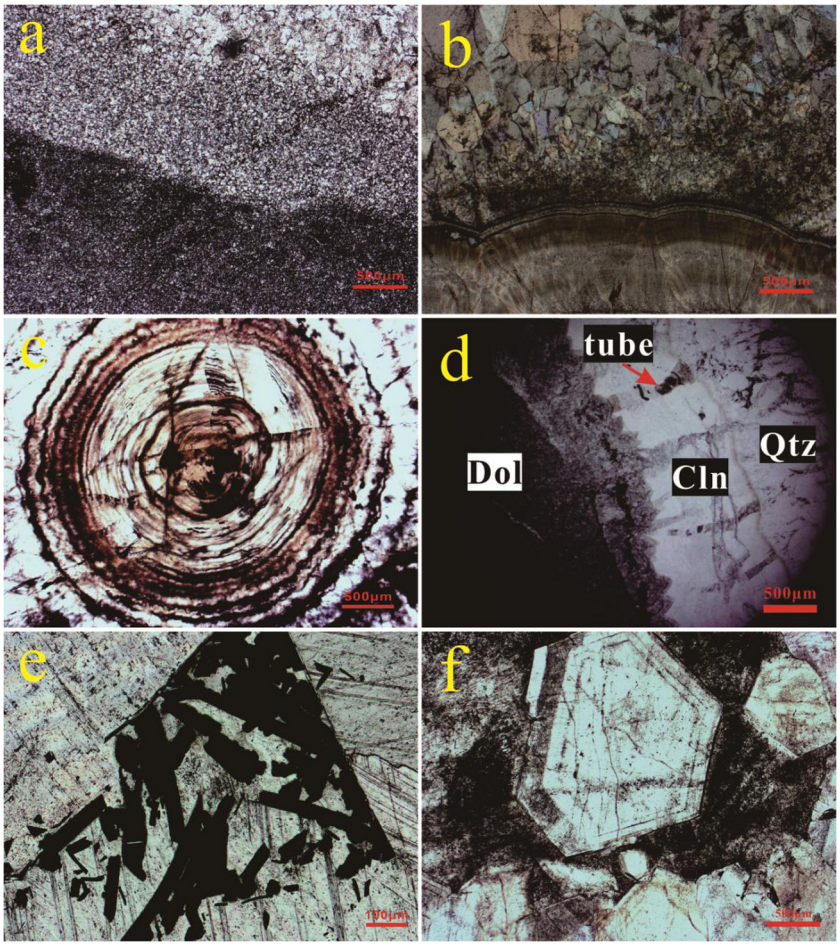

Fig. 2. (a) Plane-polarized photomicrograph of dark gray micritic dolomite gradually transitioning to grayish coarse-grained dolomite. (b) Cross-polarized photomicrograph of fibrous chalcedony gradually transitioning to euhedral quartz crystals. (c) Plane-polarized photomicrograph of oolitic structure characterized by organic-rich laminated texture in the early-stage chalcedony was observed at the Xiaofenghe section. (d) Plane-polarized photomicrograph of organic material or hydrocarbon migration tubes cross-cutting chalcedony and quartz crystals (Dol: dolostone; Cln: chalcedony; Qtz: quartz). (e) Plane-polarized photomicrograph of fractured bitumen cemented by late-stage calcite. (f) Plane-polarized photomicrograph of euhedral quartz crystal showing numerous growth zones outlined by primary fluid inclusions.

of the laminae are accompanied with abundant organic matter, as well as very fine grained (<5 μm) euhedral pyrite. Euhedral pyrite (crystal size of 15–150 μm, mostly 40–100 μm) together with sphalerite is often found in chalcedony. Moreover, some oolitic-like structures characterized by a concentrically zoned organic-rich laminated texture are also observed in chalcedony at the Xiaofenghe and Wenghui sections, which are located on the inner shelf facies and slope facies of the Yangtze Block, respectively (Fig. 2c).

Special brown[1] organic-rich "tube" textures have been observed to cross-cut chalcedony and quartz (Fig. 2d). Numerous liquid methane inclusions and hydrocarbon inclusions in quartz crystals are distributed linearly along the fissures associated with these "tubes". The later stage organic-rich calcite is accompanied with bitumen. The gray color of calcite comes from the fine bitumen dispersed in the calcite; sometimes coarse blade-like bitumen has been crushed and cemented by the late-stage gray calcite (Fig. 2e). The paragenetic sequence of minerals is summarized in Fig. 3.

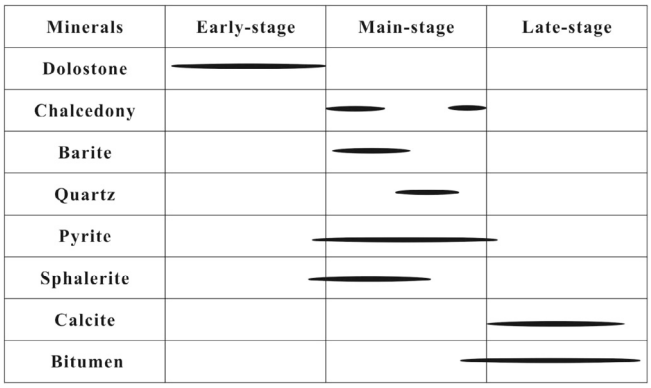

Fig. 3. Paragenetic sequences of minerals from sheet-crack cements in cap carbonates.

4.2. Types of fluid inclusion

Fluid inclusions have been observed in early-stage coarse crystalline dolomite, middle-stage quartz and late-stage calcite, but most of the inclusions in early-stage dolomite and late-stage calcite are smaller than 5 μm and cannot be used for temperature measurement. In contrast, many fluid inclusions in quartz crystals are sufficiently large for MTA. Sometimes obvious growth zones outlined by primary inclusions have been found in these quartz crystals (Fig. 2f).

[1] For interpretation of color in Fig. 2, the reader is referred to the web version of this article.

Based on Raman spectra, phases appearing at room temperature (approximately 25 °C) and phase variations during freezing-heating experiments, fluid inclusions in quartz have been classified into two types. Type I (Fig. 4a and b) are one-phase, pure liquid CH_4 fluid inclusions. These fluid inclusions are generally negative crystal or flat, elliptical, or irregular shapes; and they range in size from 8 μm × 5 μm to 29 μm × 23 μm. Most of these inclusions are distributed linearly along the fissures associated with the "tubes" structures, and some inclusions are bright blue under fluorescent light (Fig. 4e and f).

Type II (Fig. 4c and d) are two-phase liquid-rich aqueous inclusions that contain 10–20% volumetric proportions of the vapor phase at room temperature and could be homogenized to the liquid phase after heating. These inclusions are randomly isolated or distributed in group lines in quartz crystals; they may be displayed as negative crystals, or as tubular, elliptical or irregular shapes, with sizes ranging from a few microns to 20 μm. In this paper, primary Type II fluid inclusions with diameters of 8–20 μm have been selected for MTA.

4.3. Homogenization temperature (T_h) and salinity

A total of 51 data points for T_h have been observed from fluid inclusions that were clearly homogenized to a liquid phase (Table 1). The T_h of fluid inclusions falls between 83 and 256 °C (n = 51), mostly within 160–220 °C (mean, 192 °C, n = 31) (Fig. 5).

The eutectic temperatures (T_e) of some aqueous fluid inclusions are mainly around −50 to −60 °C (mean, −54 °C, n = 6; T_e is usually almost undetectable.), which would reflect a $CaCl_2$–NaCl–H_2O system. A total of 58 freezing point temperatures (T_m) have been obtained (Table 1), ranging from −20.6 to −3.9°C (n = 58). All of these T_m values exceed −21.2 °C, so the salinity can be calculated approximately using the NaCl–H_2O system (Chi and Ni, 2007). The computed salinities range from 6.3 wt.% to 22.8 wt.% NaCl equiv., and display two peaks at 6.3–8.3 wt.% and 18.0–20.8 wt.% NaCl equiv. in the salinity histogram (Fig. 5), respectively.

5. Discussion

5.1. Constraints from minerals paragenetic sequences and structure on the origin of sheet-crack

Three stages of hydrothermal fluid activities have been revealed through microscope and hand-specimen observation in sheet-crack structures: dolomitization at the early stage, silicification at the middle stage and calcitization at the late stage.

The early-stage dolomite recrystallization is characterized by regular changes of grain sizes, transitioning from micritic and fine into coarse dolomite (Fig. 2a). This change is commonly parallel with the sheet-crack. The coarse dolomites often feature ctenoid and radial textures, and barites occasionally occur between the coarse dolomites and chalcedony. Barites coating the ctenoid dolomites have been observed in field outcrops at shallow-platform facies sections such as Baizhu in Hubei Province and Jinhe in Guizhou Province; this texture has been interpreted as resulting from karstic dissolution associated with isostatic rebound (Zhou et al., 2010). The ctenoid texture could be a result of hydrothermal metasomatism of the retained aragonite after karstic processes. The temperatures of dolomite on both sides of sheet-crack cements were computed by CCIT to be 86–156 °C (Bristow et al., 2011), which indicates that the coarse dolomites have experienced a low-temperature hydrothermal process. Considering the rapid transgression after isostatic rebound, we propose that the karstic cap dolostones have been metasomatized (dolomitization of aragonite) by a low-temperature interstratal pore-brine at the beginning of the second transgression.

Chalcedony is the main mineral of sheet-crack cements, and it represents rapid precipitation from silica-rich fluids under fast cooling conditions at the beginning of the middle-stage hydrothermal activity. The dense laminated texture, consisting of interbedded pure chalcedony and organic-rich chalcedony, implies a rapid fluctuation in temperature and redox state. The distinct oolitic-like texture (Fig. 2c), observed at the Xiaofenghe (platform facies) and Wenghui (slope facies) sections, may have resulted from strong disturbances in the flow of rising thermal fluids.

There is a common mineral evolution in thick sheet-cracks, gradually transitioning from chalcedony to medium- to coarse-grained quartz (Fig. 2b), which means quartz could have grown in a quasi-equilibrium fluid with gradually stabilizing temperature. Fluid inclusions could have been trapped in quartz during this process. Typical growth zones outlined by primary inclusions have been found in euhedral quartz crystals at the Daping section in Hunan Province (Fig. 2f).

The late-stage calcitization is characterized by carbonaceous coarse calcite. Most of the calcite fills in the remaining spaces of siliceous veins or other voids, and some thin calcite veins crosscut the earlier siliceous veins. Bitumen is a typical mineral in many field outcrops of cap carbonate sections, three distribution types can be observed: fine particles dispersed in calcite, fractured coarse bitumen cemented by calcite (Fig. 2e), and coarse bitumen filled in voids of calcite. Thus, we speculate that there was a strong organic thermal decomposition event after silicification at the middle stage that lasted until the end of calcitization, which produced the abundant bitumen.

The sheet-crack structure of cap carbonate at the Jiulongwan section is mainly composed of chalcedony, quartz, calcite, and bitumen. This mineral assemblage is significantly different from that of cold seep carbonate which is mostly filled by carbonate cements (Mounji et al., 1998; Suess et al., 1999; Barbieri et al., 2004). The mineral paragenetic sequences and textures suggest that sheet-crack structure is a preserved hydrothermal fluid system after isostatic rebound and karstic dissolution.

5.2. Temperature constraint on the origin of sheet-crack

The temperatures of most cold seeps are usually close to or slightly higher than ambient seafloor temperatures (Suess, 2014). According to the temperature-depth (pressure) phase diagram for the methane hydrate system modified by Dickens et al. (1995), methane hydrate can exist in sediments where the submarine temperature is −1.5 °C and the water depth exceeds ~250 m in modern marine environments; or it could exist in sediments where bottom water temperature was ~11 °C and depth was greater than ~920 m in the late Paleocene marine environment. Given that the earth was covered by thick ice-sheets during "Snowball Earth" (Hoffman et al., 1998), we estimate that the submarine temperature was approximately 0 °C during the cap carbonate precipitation after a large amount of glacial melting. If the sheet-crack cements mainly precipitated from cold seeps, the temperature should be close to or slightly higher than the seawater temperature. The homogenization temperatures in quartz crystals of sheet-crack cements are mainly distributed within the range of 160–220 °C (mean, 192 °C, n = 31) (Fig. 5), which is distinctively higher than the submarine temperature expected for cold-seep cements.

The late-stage gray calcite is an important mineral because of its extremely ^{13}C-depleted isotope signal (down to −48‰) and its high-temperature obtained from CCIT measurements (275–476 °C, mean, 378 °C, n = 4) (Bristow et al., 2011). It is unfortunate that the fluid inclusions in the gray calcite are too small to be mea-

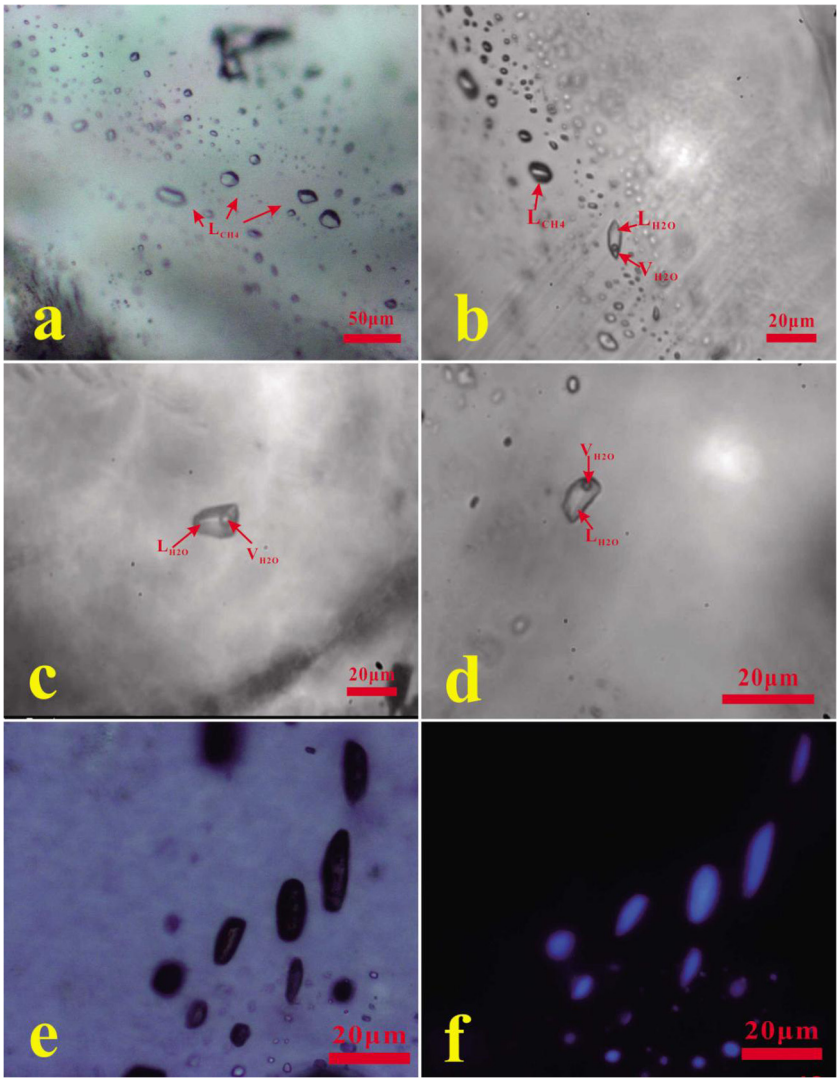

Fig. 4. Photomicrographs of fluid inclusions in quartz. (a) Type I pure CH_4 liquid inclusions in quartz. (b) Coexistence of type I CH_4 liquid inclusions and type II liquid-rich aqueous inclusions in quartz. (c, d) Type III two-phase liquid-rich aqueous inclusions in quartz. (e, f) inclusions are bright fluorescent blue under ultraviolet light. (L_{CH4} = liquid CH_4; L_{H2O} = liquid H_2O; V_{H2O} = vapor H_2O). (For interpretation of the references to color in this figure legend, the reader is referred to the web version of this article.)

sured. However, the fact that gray calcite tightly coexists with bitumen, which indicates organic thermal decomposition, provides some temperature information about the gray calcite. For instance, based on the bitumen reflectance determined, the paleotemperature of the lower Cambrian black shale series of the Niutitang Formation in northern Guizhou was estimated to be 60–250 °C (Yang et al., 2009). In the Buchan Rift, the paleotemperature of the Devonian Tabberabberan Deformation estimated from bitumen reflectance was near 200 °C (Barker and Bone, 1995). Therefore, the combination of bitumen and gray calcite indicates that there was a low- to middle-temperature thermal decomposition event.

The homogenization temperatures of fluid inclusions in quartz, CCIT temperature from the gray calcite, and the widespread existence of bitumen all suggest that there was a common hydrothermal activity during the second transgression.

5.3. Salinity constraint on the origin of sheet-crack

There are two peaks at low salinity (approximately 6.3–8.3 wt.% NaCl equiv.) and high salinity (approximately 18.0–20.8 wt.% NaCl equiv.) (Fig. 5) in the salinity histogram. This result reveals that the quartz in sheet-crack cements precipitated from a mixture of high- and low-salinity fluids. In addition, the limited but concordant eutectic temperatures (T_e) (mean −54 °C, n = 6) of those aqueous fluid inclusions reflect the more complex $CaCl_2$–NaCl–H_2O system (Samson et al., 2003).

The measured temperatures and high salinity peak of these inclusions are similar to the features of inclusions from basin brine. For example, more than 2000 fluid inclusions from fifteen typical Mississippi Valley-type (MVT) Zn-Pb deposits related to basin brine show that the means of T_h and salinity values are 122 ± 21 °C and 20.7 ± 2.6 wt.% $CaCl_2$ equiv., respectively (Basuki and Spooner, 2002). The submarine hydrothermal brine system from the Greek island of Milos in the Aegean Sea has higher salinity and higher temperature (300–325 °C) and is enriched in Na^+, Ca^{2+}, K^+, Cl^-, and SiO_2 compared to overlying seawater but is depleted in Mg^{2+} and SO_4^{2-} (Fitzsimons et al., 1997).

Thus, the precipitation of sheet-crack cements probably resulted from the mixing of hydrothermal brine ($CaCl_2$–NaCl–H_2O system) from a deep basin and circulating seawater (NaCl–H_2O system). The high-salinity peak represents hydrothermal brine

Table 1
Homogenization temperatures and salinities of fluid inclusions.

Sample no.	T_h (°C)	T_m (°C)	T_e (°C)	Slt (wt.% NaCl eq.)	Sample no.	T_h (°C)	T_m (°C)	T_e (°C)	Slt (wt.% NaCl eq.)
JLW-1	228	−4.3	nd	6.9	JLW-2	193	−7.5	nd	11.1
JLW-1	nd	−20.5	nd	22.7	JLW-2	193	−6.1	nd	9.3
JLW-1	124	−9.0	nd	12.8	JLW-2	193	nd	nd	nd
JLW-1	147	−4.2	nd	6.7	JLW-2	119	−13.7	nd	17.5
JLW-1	150	−4.2	nd	6.7	JLW-2	205	−6.8	nd	10.2
JLW-1	256	−4.8	nd	7.6	JLW-2	nd	−6.0	nd	9.2
JLW-1	161	−20.6	nd	22.8	JLW-2	186	nd	nd	nd
JLW-1	123	−14.2	nd	18.0	JLW-2	nd	−9.7	nd	13.6
JLW-1	219	−15.4	−50.0	19.0	JLW-2	nd	−4.7	nd	7.5
JLW-1	239	−15.9	nd	19.4	JLW-2	nd	−4.4	nd	7.0
JLW-1	253	−17.8	−59.3	20.8	JLW-2	nd	−4.6	nd	7.3
JLW-1	211	−17.8	nd	20.8	JLW-2	144	−17.4	nd	20.5
JLW-1	210	−15.9	−51.0	19.4	JLW-2	234	−18.8	−55.0	21.5
JLW-1	168	−7.1	nd	10.6	JLW-2	199	−16.9	nd	20.1
JLW-1	157	−6.2	nd	9.5	JLW-2	201	−4.5	nd	7.2
JLW-1	193	−7.9	nd	11.6	JLW-2	204	−4.5	−50.5	7.2
JLW-1	221	−15.2	nd	18.8	JLW-2	nd	−16.1	nd	19.5
JLW-1	137	−9.0	nd	12.8	JLW-2	193	−16.9	nd	20.1
JLW-1	171	−8.9	nd	12.7	JLW-2	nd	−18.6	nd	21.4
JLW-1	nd	−14.8	nd	18.5	JLW-2	159	−3.9	nd	6.3
JLW-1	159	−9.3	nd	13.2	JLW-2	182	−4.3	nd	6.9
JLW-1	172	−12.3	nd	16.2	JLW-2	170	−4.5	nd	7.2
JLW-1	169	−16.7	nd	20.0	JLW-2	168	−4.5	nd	7.2
JLW-1	125	−15.6	nd	19.1	JLW-2	205	−4.6	nd	7.3
JLW-1	181	−15.5	nd	19.1	JLW-2	219	−4.6	nd	7.3
JLW-1	175	−14.7	nd	18.4	JLW-2	213	−4.7	nd	7.4
JLW-1	164	−14.2	nd	18.0	JLW-2	216	−4.3	nd	6.9
JLW-1	190	−13.9	−53.0	17.7	JLW-2	101	−11.8	nd	15.8
JLW-1	183	−13.2	nd	17.1	JLW-2	83	−4.8	nd	7.6
JLW-1	179	−12.6	nd	16.5	JLW-2	107	−12.3	nd	16.2

Abbreviations: T_h = homogenization temperature; T_m = freezing point temperature; T_e = eutectic temperature; Slt = salinity; nd = not determined.

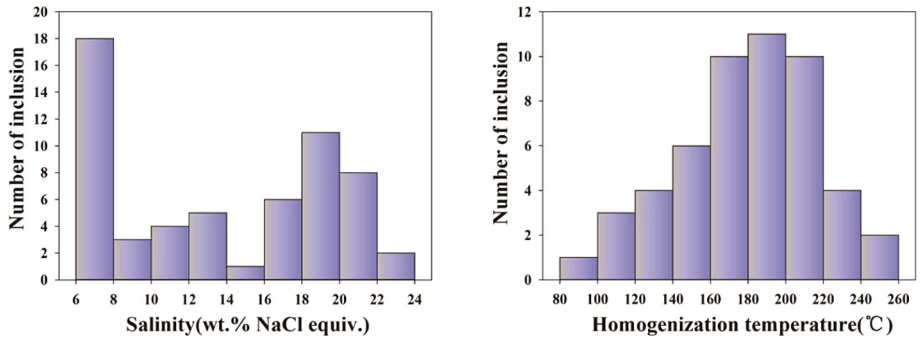

Fig. 5. Histograms of homogenization temperatures and salinities of fluid inclusions.

enriched in Fe^{2+}, Zn^{2+}, Ba^{2+} and SiO_2; the low-salinity peak represents ambient seawater enriched in SO_4^{2-}.

5.4. A model for sheet-crack origin

Fluid inclusions in quartz provide some new details (e.g., homogenization temperatures, salinity) for the post-depositional hydrothermal fluid and the hydrothermal origin of sheet-crack structure. A three-stages hydrothermal model for sheet-crack has been constructed as below:

(1) Deglaciation and the first transgression (Fig. 6a): Extensive cap carbonates were deposited at shallow water because the vast amount of Nantuo tillites flattened the preexisting platform, slope and basinal environments across the Yangtze Block (Zhou et al., 2010).
(2) Rebound and karstification (Fig. 6b): The cap carbonates were transiently uplifted due to postglacial isostatic rebound, and the ubiquitous soft-sediment deformation structures formed during concurrent seismic events (Nogueira et al., 2003). Subsequently, comprehensive karstification, which occurred both in the shallow platform and the transitional facies of the Yangtze Block (Zhou et al., 2010), further dissolved the abundant soft-sediment deformation structures into high-porosity and high-permeability strata.
(3) The second transgression, dolomitization and cementation (Fig. 6c): The high-permeability strata became a reservoir of inter-layer pore water during the second transgression at a regional or even global scale. Meanwhile the karst-genetic coarse ctenoid aragonite was altered to dolomite by inter-layer pore water. Large-scale isostatic rebound induced decompressional partial melting of the deep crust (Crowley et al., 2015). Magmatic activity adjacent to the deep faults drove the brine from down-faulted basins to circulate along the high-permeability strata in cap carbonates.

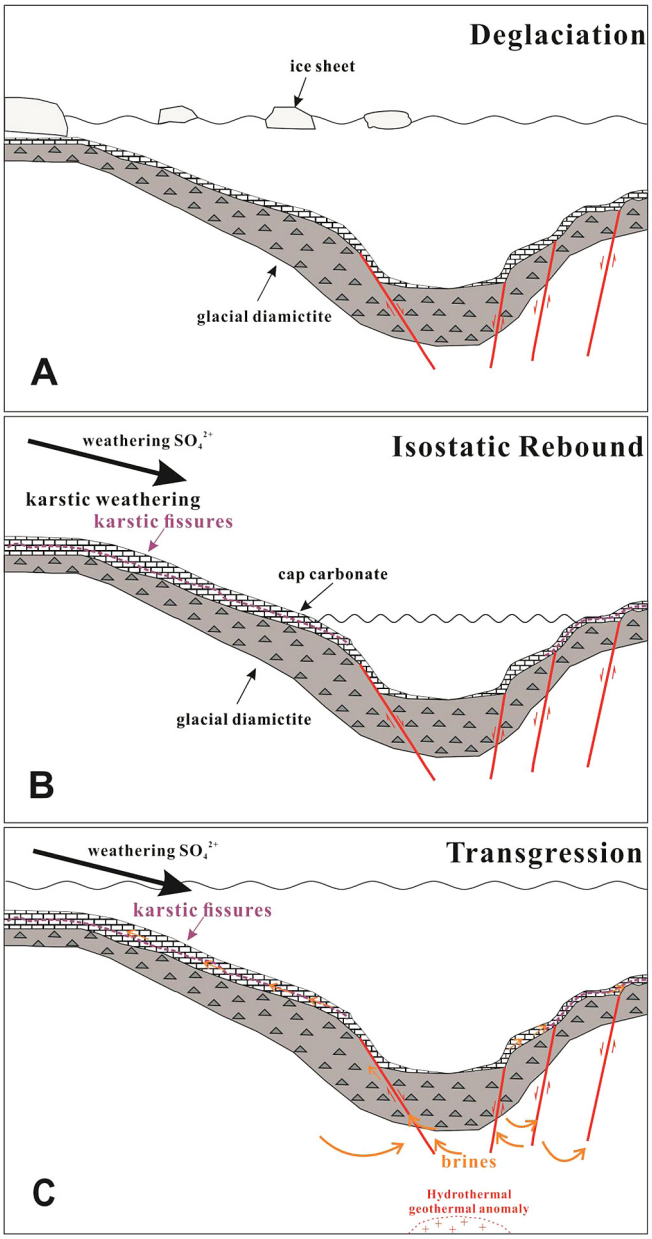

Fig. 6. The modified hydrothermal model for the sheet-crack cement structure in cap carbonates. (A) Extensive cap carbonates were deposited by the first transgression caused by deglaciation of the Snowball Earth. (B) Crust-uplift, soft-deformation and kastification had been continuously developed by the isostatic rebound. (C) Dolomitization resulted from alteration of karstic ctenoid aragonite by pore-water in the early stage of the second transgression, subsequently, silicification and calcitization should be attributed to mixture process between sea-water and the hydrothermal brine from basin settings probably driven by magmatic activity in deep-crust triggered by the isostatic rebound too.

The early hydrothermal brine was rich in SiO_2, and the late hydrothermal fluid was rich in carbonate. All of the hydrothermal activity was commonly accompanied with thermal decomposition of previously deposited organic matter. This new model successfully addresses the origin of sheet-crack structure and the paragenetic sequence of minerals, and provides direct information on the post-depositional fluid, and it is also compatible with the unified sequence of glacio-eustatic events after the termination of Marinoan glaciation (Zhou et al., 2010) and the temperature results determined by CCIT (Bristow et al., 2011).

6. Conclusions

Detailed microscopic observations and systematic analyses of fluid inclusions in the sheet-crack cements from the Jiulongwan section demonstrate that there was low- to middle-temperature hydrothermal activity after the deposition of cap carbonate. Evidence includes the following: (1) The mineral paragenetic sequence reveals three distinct stages of hydrothermal fluid activities: the early stage dolomitization, which resulted from the metasomatism of karst-genetic aragonite by inter-layer pore water; the middle stage silicification, which consisted dominantly of chalcedony precipitated under oscillatory conditions at the beginning of hydrothermal activity and, later, of quartz that grew in a stable hydrothermal fluid; and the late stage calcitization, which was comprehensively accompanied with organic thermal decomposition. (2) The homogenization temperatures of fluid inclusions in quartz mostly range from 160 to 220 °C and conform to previous CCIT results. There are two peaks, one at low salinity (approximately 6.3–8.3 wt.% NaCl equiv.) and one at high salinity (approximately 18.0–20.8 wt.% NaCl equiv.), which indicates the aforementioned mixing of hydrothermal brine from deep basins and shallow seawater. A primary conceptual model has been proposed to explain the formation of sheet-crack structure based on the inclusion data and the mineral paragenetic assemblages. Extensive cap carbonates were deposited by the first transgression caused by the fast deglaciation of the Snowball Earth. Crust-uplift, soft-deformation and kastification had been continuously developed by the isostatic rebound resulting from abruptly melting of huge-thick glaciers. Dolomitization inherited from ctenoid karstic aragonite in the early stage of the second transgression, subsequently, silicification and calcitization should be attributed to the hydrothermal brine in basin settings probably driven by magmatic activity in deep-crust triggered by the isostatic rebound too.

Conflict of interest

The authors declare that there are no conflicts of interest.

Acknowledgments

This research was funded by the National Natural Science Foundation of China (NSFC) Grants 41072054 and 41462001 awarded to Taiyi Luo and Mingzhong Zhou, respectively. We thank Chuanming Zhou for field assistance and Wenchao Su and Lin Ye for laboratory assistance in the fluid inclusions analysis.

References

Barbieri, R., Ori, G.G., Cavalazzi, B., 2004. A silurian cold-seep ecosystem from the Middle Atlas, Morocco. Palaios 19, 527–542.
Barker, C., Bone, Y., 1995. The minimal response to contact metamorphism by the Devonian Buchan Caves Limestone, Buchan Rift, Victoria, Australia. Org. Geochem. 22, 151–164.
Basuki, N., Spooner, E., 2002. A review of fluid inclusion temperatures and salinities in Mississippi Valley-type Zn-Pb deposits: identifying thresholds for metal transport. Explor. Min. Geol. 11, 1–17.
Bondar, R., 1993. Revised equation and table for determining the freezing point depression of H_2O-NaCl solution. Geochim. Cosmochim. Acta 57, 683–684.
Bristow, T.F., Bonifacie, M., Derkowski, A., Eiler, J.M., Grotzinger, J.P., 2011. A hydrothermal origin for isotopically anomalous cap dolostone cements from south China. Nature 474, 68–71.
Chi, G., Ni, P., 2007. Equations for calculation of $NaCl/(NaCl + CaCl_2)$ ratios and salinities from hydrohalite-melting and ice-melting temperatures in the H_2O-$NaCl$-$CaCl_2$ system. Acta Petrol. Sin. 23, 33–37.
Condon, D., Zhu, M., Bowring, S., Wang, W., Yang, A., Jin, Y., 2005. U-Pb ages from the neoproterozoic Doushantuo Formation, China. Science 308, 95–98.
Corkeron, M., 2007. 'Cap carbonates' and Neoproterozoic glacigenic successions from the Kimberley region, north-west Australia. Sedimentology 54, 871–903.
Crowley, J.W., Katz, R.F., Huybers, P., Langmuir, C.H., Park, S.-H., 2015. Glacial cycles drive variations in the production of oceanic crust. Science 347, 1237–1240.

Derkowski, A., Bristow, T.F., Wampler, J.M., Środoń, J., Marynowski, L., Elliott, W.C., Chamberlain, C.P., 2013. Hydrothermal alteration of the Ediacaran Doushantuo Formation in the Yangtze Gorges area (South China). Geochim. Cosmochim. Acta 107, 279–298.
Dickens, G.R., O'Neil, J.R., Rea, D.K., Owen, R.M., 1995. Dissociation of oceanic methane hydrate as a cause of the carbon isotope excursion at the end of the Paleocene. Paleoceanography 10, 965–971.
Du, W., Wang, X.L., Komiya, T., 2015. Potential ediacaran sponge gemmules from the Yangtze Gorges area in South China. Gondwana Res. 28, 1246–1254.
Fitzsimons, M.f., Dando, P.R., Hughes, J.A., Thiermann, F., Akoumianaki, I., Pratt, S.M., 1997. Submarine hydrothermal brine seeps off Milos, Greece. Observations and geochemistry. Mar. Chem. 57, 325–340.
Gammon, P.R., 2012. An organodiagenetic model for Marinoan-age cap carbonates. Sed. Geol. 243–244, 17–32.
Gammon, P.R., McKirdy, D.M., Smith, H.D., 2012. The paragenetic history of a Marinoan cap carbonate. Sed. Geol. 243, 1–16.
Hoffman, P.F., Halverson, G.P., Domack, E.W., Husson, J.M., Higgins, J.A., Schrag, D.P., 2007. Are basal Ediacaran (635 Ma) post-glacial "cap dolostones" diachronous? Earth Planet. Sci. Lett. 258, 114–131.
Hoffman, P.F., Kaufman, A.J., Halverson, G.P., Schrag, D.P., 1998. A Neoproterozoic snowball earth. Science 281, 1342–1346.
Hoffman, P.F., Macdonald, F.A., 2010. Sheet-crack cements and early regression in Marinoan (635 Ma) cap dolostones: regional benchmarks of vanishing ice-sheets? Earth Planet. Sci. Lett. 300, 374–384.
Jiang, G., Kennedy, M.J., Christie-Blick, N., 2003a. Stable isotopic evidence for methane seeps in Neoproterozoic postglacial cap carbonates. Nature 426, 822–826.
Jiang, G., Kennedy, M.J., Christie-Blick, N., Wu, H., Zhang, S., 2006a. Stratigraphy, sedimentary structures, and textures of the late Neoproterozoic Doushantuo cap carbonate in South China. J. Sediment. Res. 76, 978–995.
Jiang, G., Shi, X., Zhang, S., Wang, Y., Xiao, S., 2011. Stratigraphy and paleogeography of the Ediacaran Doushantuo Formation (ca. 635–551 Ma) in South China. Gondwana Res. 19, 831–849.
Jiang, G., Sohl, L.E., Christie-Blick, N., 2003b. Neoproterozoic stratigraphic comparison of the Lesser Himalaya (India) and Yangtze block (south China): paleogeographic implications. Geology 31, 917–920.
Jiang, G.Q., Shi, X.Y., Zhang, S.H., 2006b. Methane seeps, methane hydrate destabilization, and the late Neoproterozoic postglacial cap carbonates. Chin. Sci. Bull. 51, 1152–1173.
Kennedy, M.J., Christie-Blick, N., Sohl, L.E., 2001. Are Proterozoic cap carbonates and isotopic excursions a record of gas hydrate destabilization following Earth's coldest intervals? Geology 29, 443–446.
Liu, C., Wang, Z., Raub, T.D., Macdonald, F.A., Evans, D.A.D., 2014. Neoproterozoic cap-dolostone deposition in stratified glacial meltwater plume. Earth Planet. Sci. Lett. 404, 22–32.
McFadden, K.A., Huang, J., Chu, X., Jiang, G., Kaufman, A.J., Zhou, C., Yuan, X., Xiao, S., 2008. Pulsed oxidation and biological evolution in the Ediacaran Doushantuo Formation. Proc. Natl. Acad. Sci. 105, 3197–3202.
Mounji, D., Bourque, P.-A., Savard, M., 1998. Hydrothermal origin of Devonian conical mounds (kess-kess) of Hamar Lakhdad Ridge, Anti-Atlas, Morocco. Geology 26, 1123–1126.
Nogueira, A.C.R., Riccomini, C., Sial, A.N., Moura, C.A.V., Fairchild, T.R., 2003. Soft-sediment deformation at the base of the Neoproterozoic Puga cap carbonate (southwestern Amazon craton, Brazil): confirmation of rapid icehouse to greenhouse transition in snowball Earth. Geology 31, 613–616.
Roedder, E., Ribbe, P., 1984. Fluid Inclusions. Mineralogical Society of America, Washington, DC.
Samson, I., Anderson, A., Marshall, D.D., 2003. Fluid Inclusions: Analysis and Interpretation. Mineralogical Association of Canada.
Shen, B., Lee, C.-T.A., Xiao, S., 2011. Germanium/silica ratios in diagenetic chert nodules from the Ediacaran Doushantuo Formation, South China. Chem. Geol. 280, 323–335.
Shields, G.A., Deynoux, M., Strauss, H., Paquet, H., Nahon, D., 2007. Barite-bearing cap dolostones of the Taoudéni Basin, northwest Africa: sedimentary and isotopic evidence for methane seepage after a Neoproterozoic glaciation. Precambr. Res. 153, 209–235.
Suess, E., 2014. Marine cold seeps and their manifestations: geological control, biogeochemical criteria and environmental conditions. Int. J. Earth Sci. 103, 1889–1916.
Suess, E., Torres, M.E., Bohrmann, G., Collier, R.W., Greinert, J., Linke, P., Rehder, G., Trehu, A., Wallmann, K., Winckler, G., Zuleger, E., 1999. Gas hydrate destabilization: enhanced dewatering, benthic material turnover and large methane plumes at the Cascadia convergent margin. Earth Planet. Sci. Lett. 170, 1–15.
Wang, J., Jiang, G., Xiao, S., Li, Q., Wei, Q., 2008. Carbon isotope evidence for widespread methane seeps in the ca. 635 Ma Doushantuo cap carbonate in south China. Geology 36, 347–350.
Wang, J., Li, Z.-X., 2003. History of Neoproterozoic rift basins in South China: implications for Rodinia break-up. Precambr. Res. 122, 141–158.
Xiao, S., McFadden, K.A., Peek, S., Kaufman, A.J., Zhou, C., Jiang, G., Hu, J., 2012. Integrated chemostratigraphy of the Doushantuo Formation at the northern Xiaofenghe section (Yangtze Gorges, South China) and its implication for Ediacaran stratigraphic correlation and ocean redox models. Precambr. Res. 192–195, 125–141.
Yang, J., Yi, F., Qian, Z., 2009. Study of Paleotemperature of the lower Cambrian black shale series and their implications in Northern Guizhou province. Acta Mineral. Sin. 29, 87–94.
Yin, L., Zhu, M., Knoll, A.H., Yuan, X., Zhang, J., Hu, J., 2007. Doushantuo embryos preserved inside diapause egg cysts. Nature 446, 661–663.
Zhao, Y.Y., Zheng, Y.F., 2013. Geochemical constraints on the origin of post-depositional fluids in sedimentary carbonates of the Ediacaran system in South China. Precambr. Res. 224, 341–363.
Zhao, Y.Y., Zheng, Y.F., 2015. Geochemistry of vein and wallrock carbonates from the Ediacaran system in South China: insights into the origins of depositional and post-depositional fluids. Chem. Geol. 404, 71–87.
Zhao, Z.Q., Xing, Y.S., Ma, G.G., Chen, Y.Y., 1985. Biostratigraphy of the Yangtze Gorge Area (1) Sinian. Geological Publishing House, Beijing.
Zhou, C., Bao, H., Peng, Y., Yuan, X., 2010. Timing the deposition of ^{17}O-depleted barite at the aftermath of Nantuo glacial meltdown in South China. Geology 38, 903–906.
Zhou, C., Jiang, S., Xiao, S., Chen, Z., Yuan, X., 2012. Rare earth elements and carbon isotope geochemistry of the Doushantuo Formation in South China: implication for middle Ediacaran shallow marine redox conditions. Chin. Sci. Bull. 57, 1998–2006.
Zhou, C., Xiao, S., 2007. Ediacaran δ^{13}C chemostratigraphy of South China. Chem. Geol. 237, 89–108.